This article was downloaded by:
On: *25 January 2011*
Access details: *Access Details: Free Access*
Publisher *Taylor & Francis*
Informa Ltd Registered in England and Wales Registered Number: 1072954 Registered office: Mortimer House, 37-41 Mortimer Street, London W1T 3JH, UK

Liquid Crystals
Publication details, including instructions for authors and subscription information:
http://www.informaworld.com/smpp/title~content=t713926090

Optical Bragg reflection from the TGBA phase

Pascal Hubert

Online publication date: 06 August 2010

To cite this Article Hubert, Pascal(1999) 'Optical Bragg reflection from the TGBA phase', Liquid Crystals, 26: 9, 1379 — 1386
To link to this Article: DOI: 10.1080/026782999204057
URL: http://dx.doi.org/10.1080/026782999204057

PLEASE SCROLL DOWN FOR ARTICLE

Full terms and conditions of use: http://www.informaworld.com/terms-and-conditions-of-access.pdf

This article may be used for research, teaching and private study purposes. Any substantial or systematic reproduction, re-distribution, re-selling, loan or sub-licensing, systematic supply or distribution in any form to anyone is expressly forbidden.

The publisher does not give any warranty express or implied or make any representation that the contents will be complete or accurate or up to date. The accuracy of any instructions, formulae and drug doses should be independently verified with primary sources. The publisher shall not be liable for any loss, actions, claims, proceedings, demand or costs or damages whatsoever or howsoever caused arising directly or indirectly in connection with or arising out of the use of this material.

LIQUID CRYSTALS, 1999, VOL. 26, NO. 9, 1379–1386

Optical Bragg reflection from the TGBA phase

PASCAL HUBERT

Dipartimento di Fisica del Politecnico di Torino and Istituto Nazionale di Fisica della Materia, Corso Duca degli Abruzzi, 24, 10129 Torino, Italy;
e-mail: hubert@polito.it

(*Received 19 December 1998; accepted 19 March 1999*)

We have studied theoretically the reflection band properties of the twist grain boundary A phase (TGBA). A 4×4 matrix approach for the electromagnetic wave propagation is used. At normal incidence, simple analytical expressions are found, while at oblique incidence numerical methods have to be used since no analytical solution is available. The chart of stability of the propagating waves and the reflection spectra are given and discussed. No evidence of the incommensurability properties of the TGBA phases can be found optically. However, the analysis of the output polarization within the Bragg reflection band, on thick enough samples, allows us to determine the physical parameters characterizing the TGBA phase. In particular conditions, we can get the rotation $\Delta\varphi$ between two homogeneous slabs and the total optical phase ϕ of one slab. When $\Delta\varphi$ and ϕ go to zero, the optical properties of the TGBA phase become identical to those of the cholesteric phase. The essential difference appears when $\Delta\varphi$ and ϕ are increased; an infinite number of reflection bands forms each Bragg reflection order, due to the periodicity of the TGBA parameters.

Downloaded At: 19:09 25 January 2011

1. Introduction

Helical structures are traditional entities in liquid crystal (LC) materials. Ordinary LC phases like the chiral smectic C phase and the cholesteric phase are wisely used for theoretical and applied studies. During the last decade, new structures called twist grain boundary (TGB) phases have been discovered in chiral compounds. Actually, one can identify three different phases which have been named TGBA [1], TGBC [2] and TGBC* [3]. The first two are periodic in one direction, while the last one is periodic in two orthogonal directions and will not be considered in this paper. The structural properties of TGB phases were first formulated in the theoretical work of Renn and Lubensky (RL) [4, 5] based on the formal analogy introduced by de Gennes [6] between the smectic phase in LCs and the Abrikosov phase in type II superconductors. Figure 1 shows the structure proposed by Renn and Lubensky for the TGBA phase which is confirmed by many experiments [7–9]. Two successive smectic slabs of thickness l_b are discretely rotated at an angle $\Delta\varphi$ along a direction parallel to the smectic planes, say z. The interface between each slab (grain boundary) is constituted of a grating of screw dislocations spaced at a regular distance l_d. These dislocations are not observable optically and the TGBA phase shows then a helical superstructure in the z-direction which can be characterized by its reflection spectra. For the TGBC phase, it has recently been shown that the optic axis of the smectic slab is orthogonal to the helix direction [2]. The induced biaxiality is generally negligible and the TGBC structure is then optically equivalent to that of the TGBA phase.

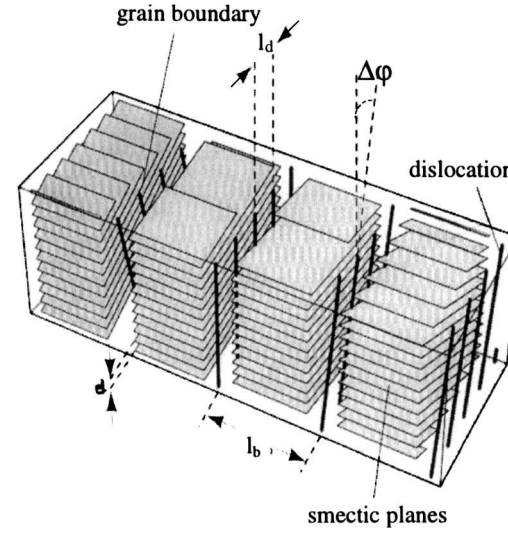

Figure 1. General view of the TGB structure. The smectic slabs of thickness l_b are discretely rotated by an angle $\Delta\varphi$ along the z-direction and between each slab (grain boundary) a grating of screw dislocations spaced at a regular distance l_d takes place.

The information which is provided by the Bragg reflection band may be analysed, the chart of stability allowing us to perform a deep analysis of the periodic medium. Up to now, only a few studies have been

Journal of Liquid Crystals ISSN 0267-8292 print/ISSN 1366-5855 online ©1999 Taylor & Francis Ltd
http://www.tandf.co.uk/JNLS/lct.htm
http://www.taylorandfrancis.com/JNLS/lct.htm

performed on the optical properties of the TGB phases [10], even though they are similar to those of Reusch's piles [11] or of Solc filters [12]. The aim of this work is to study these properties in order to find the structural parameters characterizing the TGBA phase. To this purpose, we first review the general theory of electromagnetic wave propagation based on the 4×4 matrix approach (§2). An analytical description of the wave propagation in TGBA phases at normal incidence is then developed (§3). Finally, before giving concluding remarks (§5), we discuss the chart of stability which is obtained for the most general case of oblique incidence (§4).

2. Theory

Let us consider here a geometry where the helix axis of the superstructure is orthogonal to the boundaries of the sample, giving rise to a stratified medium. In this geometry, as is well known, the electromagnetic wave propagation can be solved using a standard 4×4 matrix approach obtained by a suitable rearrangement of the Maxwell equations introduced by Berreman [13] for LC optics. For a monochromatic wave of wavelength λ propagating along the z-direction, we only have to consider the z-dependence of the field components, because of the complete translational symmetry properties along all the directions orthogonal to the z-axis. The propagation equation to the β-vector, $\beta=(E_x, H_y, E_y, -H_x)^t$, (t for transpose) containing the components of the electromagnetic field, is then written as

$$\frac{\partial\beta}{\partial z}=ik_0\boldsymbol{B}\beta \tag{1}$$

where $\boldsymbol{B}$ is the 4×4 Berreman matrix and $k_0=2\pi/\lambda$. In the case of a homogeneous medium, the Berreman matrix is z-independent and the solution of equation (1) is $\beta(z)=\boldsymbol{U}_\beta(z-z_0)\beta(z_0)$, where $\boldsymbol{U}_\beta(z-z_0)$ is the β transfer matrix over the thickness $(z-z_0)$ and is written as

$$\boldsymbol{U}_\beta(z-z_0)=\exp[ik_0\boldsymbol{B}(z-z_0)]. \tag{2}$$

It is usually convenient to work with the so-called α-vectors, which are made up of the amplitudes of four polarized plane waves propagating in the medium. They correspond to the ordinary and extraordinary waves which propagate forwards and backwards. They are defined such that

$$\beta=\boldsymbol{T}\alpha \tag{3}$$

where $\boldsymbol{T}$ is the 4×4 matrix whose elements t_{ij} are the i^{th} component of the Berreman eigen vector β_j. The propagation matrix for the α-vectors is then $\boldsymbol{U}_\alpha=\boldsymbol{T}^{-1}\boldsymbol{U}_\beta\boldsymbol{T}$.

The transmittance tr and the reflectance rf are obtained by applying the projection matrices $\boldsymbol{P}_+$, $\boldsymbol{P}_-$, onto $\boldsymbol{U}_\alpha$ which give the subspaces of the forward and backward propagating waves, respectively [14]. We have

$$tr=(\boldsymbol{P}_+\,\boldsymbol{U}_\alpha\boldsymbol{P}_+^{-1})^{-1}$$

and

$$rf=(\boldsymbol{P}_-\,\boldsymbol{U}_\alpha^{-1}\boldsymbol{P}_+^{-1})[(\boldsymbol{P}_-\,\boldsymbol{U}_\alpha^{-1}\boldsymbol{P}_-^{-1})]^{-1}. \tag{4}$$

The electromagnetic wave within the medium can propagate or be evanescent. These two electromagnetic states can be referred to as the stable and unstable solution, respectively. Further, the chart of stability which gives the instability properties as a function of the parameters of the system is found by analysing the transfer matrix of the periodic structure, $\boldsymbol{U}_\alpha$. To that purpose, an analysis on the eigenwaves of the equivalent Berreman-matrix [15] or a resolution of the Maxwell equations according to the Bloch–Floquet theorem [16] can be made. However, in our case the stable regions of the system are found by analysing the properties of the four complex eigenvalues $r_j\,(j=1,\ldots,4)$, of the transfer matrix $\boldsymbol{U}_\alpha$. These eigenvalues are obtained analytically and numerically for normal incidence and oblique incidence, respectively. If $|r_j|>1$ or $|r_j|<1$ the wave is an increasing or a decreasing evanescent wave, respectively, and for $|r_j|=1$ the wave is propagating. If two of the four proper waves do not propagate, a selective reflection takes place (Bragg reflection), while with four non-propagating waves, a total reflection occurs which does not fulfill the classical Bragg condition.

3. Normal incidence: secular equation and chart of stability

In a first approximation, within the stratified medium, the grain boundaries are not optically observable and their thickness is neglected. Within this approximation, the same contains a number N of uniaxial slabs of thickness l_b, which are stacked successively with a rotation $\Delta\varphi$ between each of them, the local optical axis being parallel to the boundary planes. Further, we consider a plane wave incident on this set of N homogeneous layers separated by $N+1$ planes at $z=z_n$ $(n=0,1,\ldots,N)$, with the aim of finding out the analytic expression of the proper wave vector, corresponding to the eigenwave, within the periodic medium. We write the α-vectors at the interface between two successive layers, $(n-1)$ and (n), as shown in figure 2, as

$$\alpha(z_n^-)=(i_e, r_e, i_o, r_o)^t,\quad \alpha(z_n^+)=(t_e, r'_e, t_o, r'_o)^t \tag{5}$$

where i, r, t correspond to the incident, reflected and transmitted wave of the n plane, r' corresponds to the reflected wave of the $n+1$ plane, and the indices e, o correspond to the extraordinary and ordinary wave, respectively. The continuity of the tangential components

Downloaded At: 19:09 25 January 2011

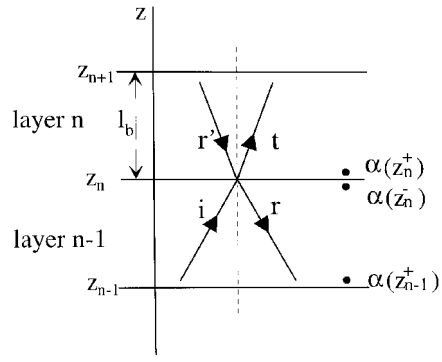

Figure 2. Incident, reflected and transmitted wave in the stratified medium.

of the vectors **E** and **H** is expressed by the relation $\beta(z_n^+) = \beta(z_n^-)$ and with equation (3) we obtain

$$\alpha(z_n^+) = \boldsymbol{T}_n^{-1}\,\boldsymbol{T}_{n-1}\,\alpha(z_n^-) \tag{6}$$

where $\boldsymbol{T}_{n-1}$, $\boldsymbol{T}_n$ are the $\boldsymbol{T}$-matrix of the layers $(n-1)$ and (n), respectively. From equations (2) and (6), the transfer matrix for the α-vectors between the planes $z = z_{n-1}^+$ and $z = z_n^+$ [corresponding to the $(n-1)$-layer and its second interface] is written as

$$\boldsymbol{U}_{n-1} = \boldsymbol{R}_{n,n-1}\boldsymbol{P}_{n-1} \tag{7}$$

with $\boldsymbol{R}_{n,n-1} = \boldsymbol{T}_n^{-1}\,\boldsymbol{T}_{n-1}$ and where $\boldsymbol{P}_{n-1}$ is a diagonal transfer matrix for the homogeneous slab $(n-1)$. At normal incidence, very simple expressions for $\boldsymbol{T}_n$ and $\boldsymbol{P}_n$ are found as follows:

$$\boldsymbol{P}_n = \begin{bmatrix} \exp(\mathrm{i}\phi_e) & 0 & 0 & 0 \\ 0 & \exp(-\mathrm{i}\phi_e) & 0 & 0 \\ 0 & 0 & \exp(\mathrm{i}\phi_o) & 0 \\ 0 & 0 & 0 & \exp(-\mathrm{i}\phi_o) \end{bmatrix} \tag{8}$$

and

$$\boldsymbol{T}_n = \begin{bmatrix} \dfrac{\cos\varphi_n}{\sqrt{n_e}} & \dfrac{\cos\varphi_n}{\sqrt{n_e}} & -\dfrac{\sin\varphi_n}{\sqrt{n_o}} & -\dfrac{\sin\varphi_n}{\sqrt{n_o}} \\ \cos\varphi_n\sqrt{n_e} & -\cos\varphi_n\sqrt{n_e} & -\sin\varphi_n\sqrt{n_o} & \sin\varphi_n\sqrt{n_o} \\ \dfrac{\sin\varphi_n}{\sqrt{n_e}} & \dfrac{\sin\varphi_n}{\sqrt{n_e}} & \dfrac{\cos\varphi_n}{\sqrt{n_o}} & \dfrac{\cos\varphi_n}{\sqrt{n_o}} \\ \sin\varphi_n\sqrt{n_e} & -\sin\varphi_n\sqrt{n_e} & \cos\varphi_n\sqrt{n_o} & -\cos\varphi_n\sqrt{n_o} \end{bmatrix} \tag{9}$$

where $\varphi_n = (n-1)\Delta\varphi$, $\phi_e = k_0 n_e l_b$, $\phi_o = k_0 n_o l_b$, and n_e and n_o are the local extraordinary and ordinary refractive indices of the uniaxial medium, respectively. As expected, $\boldsymbol{P}_n$ is independent of n. For lossless media, the orthogonality relations taken from ref. [17] between the columns of the $\boldsymbol{T}$-matrix allows us easily to obtain the inverse of the matrix $\boldsymbol{T}_n$ and then the matrix $\boldsymbol{R}_{n,n-1} = \boldsymbol{T}_n^{-1}\,\boldsymbol{T}_{n-1}$ becomes

$$\boldsymbol{R}_{n,n-1} = \begin{bmatrix} \cos\Delta\varphi & 0 & A\sin\Delta\varphi & B\sin\Delta\varphi \\ 0 & \cos\Delta\varphi & B\sin\Delta\varphi & A\sin\Delta\varphi \\ -A\sin\Delta\varphi & B\sin\Delta\varphi & \cos\Delta\varphi & 0 \\ B\sin\Delta\varphi & -A\sin\Delta\varphi & 0 & \cos\Delta\varphi \end{bmatrix} \tag{10}$$

with

$$A = \frac{1}{2}\left[\left(\frac{n_e}{n_o}\right)^{1/2} + \left(\frac{n_o}{n_e}\right)^{1/2}\right]$$

and

$$B = \frac{1}{2}\left[\left(\frac{n_e}{n_o}\right)^{1/2} - \left(\frac{n_o}{n_e}\right)^{1/2}\right].$$

Since the rotation $\Delta\varphi$ between two successive slabs and the slab thickness l_b are constants, all the matrices $\boldsymbol{U}_n$ are identical to $\boldsymbol{U}_1 = \boldsymbol{R}_{1,0}\boldsymbol{P}_0$. Therefore, the propagating matrix $\boldsymbol{U}_\alpha$ for the whole sample of thickness d confined between two semi-infinite isotropic media (as for instance glass) is

$$\boldsymbol{U}_\alpha = \boldsymbol{T}_g^{-1}\boldsymbol{P}_0(\boldsymbol{U}_1)^{N-1}\boldsymbol{T}_g \tag{11}$$

where $\boldsymbol{T}_g$ is the $\boldsymbol{T}$-matrix for the isotropic media. As equation (11) shows, the optical properties of the whole sample are governed by the properties of the $\mathbf{U}_1$ matrix. The four eigenvalues of $\boldsymbol{U}_\alpha$ are $r_j = \exp(\mathrm{i}k_j l_b)$, where k_j plays the role of a wave vector. Then, if r is one of $\{r_j\}$, we easily prove that $1/r$ is also an eigen value of $\boldsymbol{U}_1$. With $y = r + 1/r$, the secular equation of $\boldsymbol{U}_1$ is written as

$$g(y) = y^2 + ay + b \tag{12}$$

where $a = -2\cos\Delta\varphi(\cos\phi_e + \cos\phi_o)$ and

$$b = 2\cos^2\Delta\varphi(1 + \cos\phi_e\cos\phi_o) + 2\cos\phi_e\cos\phi_o - \left(\frac{n_e}{n_o} + \frac{n_o}{n_e}\right)\sin^2\Delta\varphi\sin\phi_e\sin\phi_o - 2.$$

The four solutions of equation (12) together with $y = r + 1/r$ are simple and can be written as

$$r_{\pm}^{1,2} = \frac{y_{1,2} \pm (y_{1,2}^2 - 4)^{1/2}}{2} \quad \text{with} \quad y_{1,2} = \frac{-a \pm (a^2 - 4b)^{1/2}}{2}. \tag{13}$$

From equation (13) it is easy to find the proper wave vectors k_j. As we see from above, a real k corresponds

Downloaded At: 19:09 25 January 2011

to a propagating wave (*stable solution*) and a complex or purely imaginary k to an evanescent wave (*unstable solution*). In figure 3, we give the chart of stability as a function of $\Delta\varphi$ and ϕ, which is the mean phase of one homogeneous slab, $\phi = (\phi_e + \phi_o)/2$, (with $n_e = 3$ and $n_o = 2$). The loci of the white, grey and black points correspond to the cases where there are four, two and zero propagating waves, respectively. A thick enough sample gives total reflection within the black regions and selective reflection within the grey regions. Three reflection bans are observed. Let us consider the instability regions ① and ②. For our analysis it is convenient to take the usual definition of the slab thickness l_b, and the pitch p (or pseudo-pitch when the ratio $2\pi/\Delta\varphi$ is not an integer, cf. the following section) of the TGB structures [4, 5] as:

$$l_b = \frac{\lambda}{2\pi\tilde{n}}\phi \quad \text{and} \quad p = \frac{2\pi}{\Delta\varphi}l_b \tag{14}$$

where $\tilde{n} = (n_e + n_o)/2$ is the mean refractive index. With these definitions, it is easy to see that the first unstable band ① of figure 3 occurs when $\Delta\varphi/\phi = \lambda/(\tilde{n}p) \approx 1$, which corresponds to the Bragg reflection. In fact in the limits $\Delta\varphi \to 0$ and $\phi \to 0$, a uniform rotation of the optic axis is realized and the considered instability region of the TGBA phase corresponds to the well known Bragg reflection band in cholesterics.

The angle $\Delta\varphi$ is defined modulus π, since it gives the direction of the optic axis of the slab. It follows that we obtain an infinite number of instability regions in the $\Delta\varphi$ direction. With this condition, the second reflection band ② corresponds also to the first order Bragg condition, but it describes the optical properties of a left circular helix ($\Delta\varphi < 0$) if the previous structure was right handed ($\Delta\varphi > 0$). These properties are confirmed in figures 4(*a*) and 4(*b*) where a 2D-surface plot of the transmittance for a dextrogyre (right) and levogyre (left) incident polarization is given, respectively. The intensity is represented with a brightness scale (black and white corresponding to intensity values of 0 and 1, respectively) as a function of ϕ and $\Delta\varphi$, for a monochromatic wave ($\lambda = 0.6328\ \mu$m), and the sample data $d = 10\ \mu$m, $p = 0.3\ \mu$m, $n_o = 1.5$ and $n_e = 1.66$. This interference pattern is also found periodically along the ϕ-direction due to the definition of ϕ in modulus 2π [18].

The third reflection band ③ appearing in the chart of stability (see figure 3) is independent of the polarization state as shown in figure 4. It occurs around $\phi = \pi$, and is evidently due to the fact that the waves reflected by any pair of boundary planes add coherently. It can also correspond to the Bragg reflection of a medium of period l_b, when the optical path along one period is equal to a half wavelength, despite the fact that here the period of the superstructure is different. If l_b is in the visible range, this property allows us to obtain the value of the slab thickness by an optical method. However, the fluctuations of the l_b value which exist at any equilibrium state, within the TGB structures, can seriously destroy this interference pattern.

Figure 4(*c*) represents a 2D-surface plot of the transmission intensity between parallel polarizers as a function of ϕ and $\Delta\varphi$. A very large range of the pitch values is obtained, and for $\Delta\varphi < 0.13\phi$, p is greater than $10\ \mu$m. In these long pitch regions, the polarization follows the orientation of the slab director: we are in the Mauguin limit. The observed zero-transmittance corresponds then to a σ-polarized output wave. This limit is obviously present in the cholesteric phase which is found by assuming the parameters of the TGBA phase, $\Delta\varphi$ and ϕ, to be close to zero [19].

In our analysis, the TGBA structures are considered to be a discrete packing of homogeneous slabs. Further, one of the most important problems which has to be solved is connected with the commensurability of the medium: i.e. to what extent an optical analysis can differentiate the commensurable and the incommensurable structures of the phase. By setting the rotation angle to $\Delta\varphi = 2\pi/a$, three cases can be distinguished: (a) a is an integer, (b) a is rational, (c) a is irrational. The medium is commensurable in the first two cases while it is incommensurable in the last case. It follows obviously that the period of the system is al_b for (a), greater than al_b for (b) and infinite for (c). The reflection bands of our system should follow this variation of the pitch.

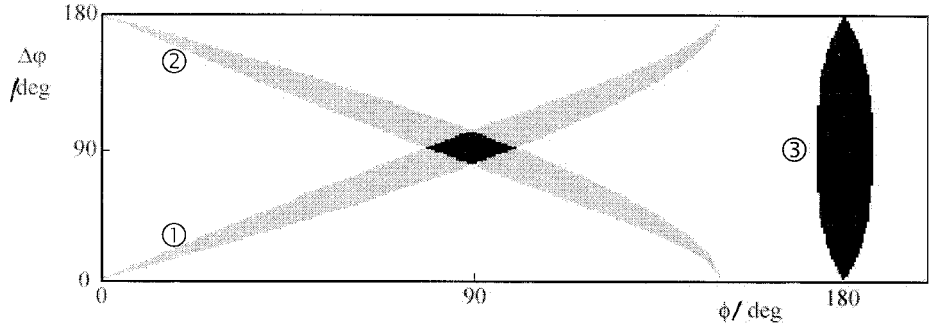

Figure 3. Chart of stability on one slab at normal incidence as a function of the parameters of the TGBA phase $\Delta\varphi$ and ϕ ($n_e = 3$ and $n_o = 2$). The white, gray and black regions correspond to 4, 2, and 0 propagating waves.

Downloaded At: 19:09 25 January 2011

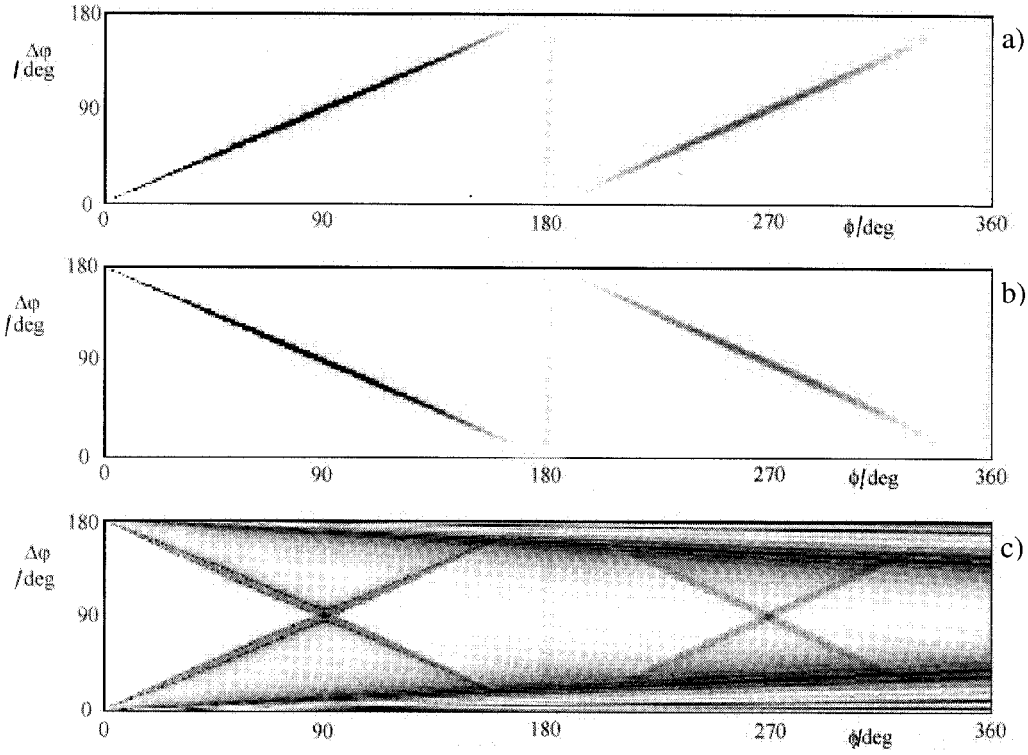

Figure 4. Transmission for (*a*) a left, (*b*) a right circular polarization of the incident light, and (*c*) intensity of the ππ transmission of a normally linear incident wave as a function of $\Delta\varphi$, ϕ ($n_e = 1.66$, $n_o = 1.5$, $\lambda = 0.6328\,\mu m$ and $d = 10\,\mu m$). The brightness scale is related to the intensity value of the transmittance which is equal to 1 and 0 for white and black, respectively.

Downloaded At: 19:09 25 January 2011

However, the chart of stability obtained over one slab is a continuous function of the TGB parameters. This means that the position of the reflection band and the actual period of the medium are fully unrelated quantities. This point can be explained by the fact that the reflection band is found by making use of a rotating reference frame, as usual for helical structures. The imaginary part of the wave vector, giving the instability, is then obtained for a medium which in any case appears periodic with the period $p = 2\pi l_b/\Delta\varphi = a l_b$. The medium is then defined with a true period in the (a) case and with a pseudo-period in cases (b) and (c). This means that we cannot predict the incommensurable properties of the TGB phases directly by analysing the instabilities of one slab at normal incidence.

In the laboratory frame, the real part of the wave vector and the corresponding eigen vector are modified when a variation of the TGB parameters occurs. This suggests that we can find some other optical properties which in particular are sensible to a small $\Delta\varphi$ variation. This is shown in figures 5(*a*) and 5(*b*) which present the reflection spectra and the optical rotation, respectively, of two closed structures: the S1-structure with $\Delta\varphi = \Delta\varphi_0 = 18°$ and the S2-structure with $\Delta\varphi = \Delta\varphi_0 + \delta\varphi$ with $\delta\varphi \approx 0.03°$. The slight change in the rotation angle $\Delta\varphi$ does not change the Bragg peak position, meaning that the periodicity of the system remains the same. On the other hand, some great changes happen in the rotation of the transmitted beam which is elliptically polarized. In a first approximation, the variation of the rotation angle with $\delta\varphi$ is just given by $N\delta\varphi$ (where N is the number of TGB blocks in the sample). This $\Delta\varphi$-sensibility is present for any choice of $\Delta\varphi_0$. Moreover, ever more critical effects are observed when the rotation angle $\Delta\varphi_0$ increases. Figures 5(*c*), and 5(*d*) show the reflection spectra and the optical rotation for $\Delta\varphi_0 = 90°$. For the S1-structure, the optical axis of each slab is orthogonal to the next and the transmitted polarization is always linear, while for the S2-structure the polarization properties can be quasi-circular at the Bragg peak. This last effect is independent of the sample thickness, because the output polarization is strongly depolarized. However, for smaller $\Delta\varphi$ angles, this effect becomes more observable as the thickness increases, as expected.

4. TGBA phases at oblique incidence

The analysis made in §3 is not allowed for oblique incidence, because all the transfer matrices $\boldsymbol{U}_n$ of one slab are not equal. Then, it is no longer possible simply to have the transfer matrices for the whole sample $\boldsymbol{U}_\beta$ as a power of the matrix $\boldsymbol{U}_1$ as in equation (11).

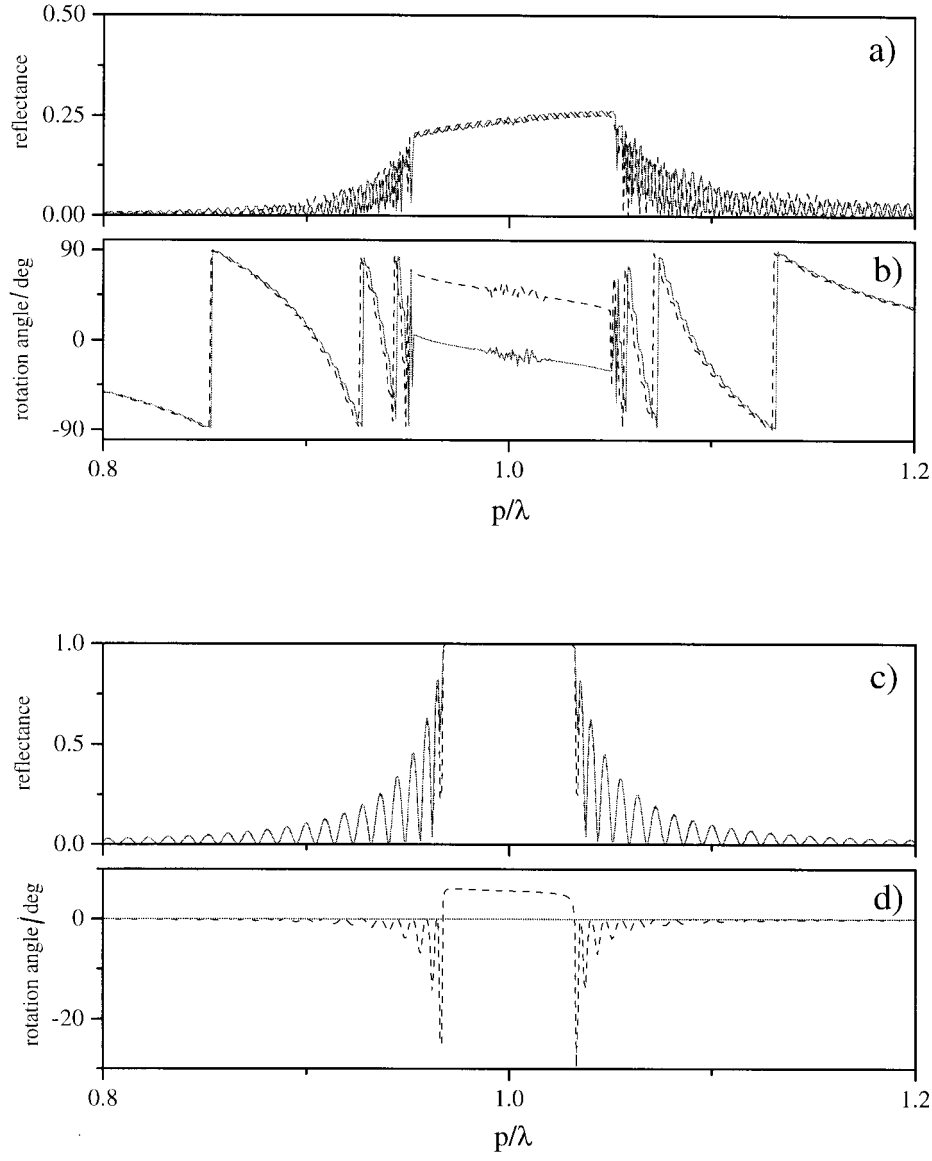

Figure 5. (a, c) $\pi\pi$ reflectance and (b, d) rotation angle of the main axis of the output polarization as a function of p/λ with $n_e = 1.66$, $n_o = 1.5$ and $p = 0.3\,\mu$m. Full line elates to the S1-structure ($\Delta\varphi = \Delta\varphi_0$) and dashed line to the S2-structure ($\Delta\varphi = \Delta\varphi_0 + \delta\varphi$). For ($a$) and ($b$), $\Delta\varphi_0 = 18°$, $\delta\varphi \approx 0.03°$ and sample thickness $d = 100p$; for (c) and (d), $\Delta\varphi_0 = 90°$, $\delta\varphi \approx 0.03°$ and $d = 50p$.

Downloaded At: 19:09 25 January 2011

Moreover, an analytical solution of the characteristic equation of $\boldsymbol{U}_\beta$ at oblique incidence does not actually exist unfortunately, and we have to solve it numerically.

Let us consider a dielectric tensor which describes a local uniaxial medium with the optic axis orthogonal to the helix axis. With no limiting assumption that the incident beam must be in the xy-plane, the Berreman matrix for the n slab of thickness l_b becomes

$$\boldsymbol{B}_n(\varphi_n) = \begin{bmatrix} 0 & b_{12} & 0 & 0 \\ a_0 + a_1 \cos 2\varphi_n & 0 & a_1 \sin 2\varphi_n & 0 \\ 0 & 0 & 0 & 1 \\ a_1 \sin 2\varphi_n & 0 & b_0 - a_1 \cos 2\varphi_n & 0 \end{bmatrix} \tag{15}$$

where $a_0 = (\varepsilon_o + \varepsilon_e)/2$, $a_1 = (\varepsilon_e - \varepsilon_o)/2$, $b_0 = a_o - p_0^2$, $b_{12} = 1 - p_0^2 \varepsilon_o^{-1}$, $p_0 = n_g \sin\theta_g$ (n_g, θ_g are the refractive index and the incident angle within the isotropic medium, respectively) and φ_n is the azimuthal orientation of the optic axis within the n-slab. We recall that this method is the one used to describe a cholesteric phase where ε_o and ε_e are the local ordinary and extraordinary dielectric constants, respectively. If N is the number of slabs within the whole sample, by following equation (2) the transfer matrix $\boldsymbol{U}_\beta$ is

$$\boldsymbol{U}_\beta = \prod_{n=1}^{N} \exp[\mathrm{i}k_0 \boldsymbol{B}_n(\varphi_n) l_b]. \tag{16}$$

For the incommensurate structure a true period of the medium does not exist and the computation is rather

long because it must be done with the N slabs of the sample. Further, we will only consider true periodic structures (*commensurable*) in which the transfer matrix can be evaluated over one pitch containing N_p slabs.

Figure 6 shows some charts of stability constructed numerically for the TGBA phase at oblique incidence. They are represented as a function p/λ and p_0^2, for different rotation angles $\Delta\varphi = 2\pi/N_p$ with $N_p = 20$(a), 4(b), 3(c) and the same parameters as in figure 3. Beside the chart of stability, we show the rotation θ of the main axis of the output polarization for an incidence angle of 45°. For small values of the rotation angle $\Delta\varphi$ [cf. figure 6(*a*)], our simulations give similar charts of stability to those obtained for cholesterics [16], as expected. They show all types of instability within the reflection band as the total and the Bragg reflection. Further, it can be seen that all the reflection bands of order higher than one disappear when the incidence angle goes to zero. This agrees with the well known result which allows only one single band reflection at normal incidence for cholesterics. Since the p/λ range in figure 6(*a*) corresponds to $\phi < \pi/2$, only one of the bands given in figure 3 appears. As the rotation angle $\Delta\varphi$ increases, figures 6(*b*) and 6(*c*), the ϕ range increases and a second reflection band appears. This band corresponds to another inversion of the optical rotation and can consequently correspond to the Bragg condition. This property has the same origin as the multiple Bragg peak of order one shown previously and is therefore due to the periodical properties of our system.

Downloaded At: 19:09 25 January 2011

5. Conclusions

In this paper, we have studied some optical properties of the TGBA phase at normal and oblique incidence by analysing the instabilities of the progagating waves and the reflection bands. The homeotropic geometry is described and the Berreman 4×4 matrix approach is used. For a normally incident beam, the transfer matrix and the secular equation for one slab of the TGBA structures are found analytically. The discussion of the commensurable properties of these structures is a false debate since no links have been established between the true period of the medium and the reflection band patterns. However, with a fine analysis of the Bragg peak in the visible range, we can obtain the structural parameters of the TGBA phase. This determination is allowed for large pitch and rotation angle. However, that case it is not yet compatible with the actual parameters of the TGBA compounds. For a short period, only the pitch value and the birefringence can be obtained because the block size is too small to be seen optically. For oblique incidence, the 4×4 matrix numerical approach is enough to find all kinds of instabilities of the propagating waves in the sample. We then described the chart of stability obtained in terms of Bragg and total reflection bands. The general properties of the TGBA phase are very similar to those of the cholesteric phase when the parameters $\Delta\varphi$ and ϕ go to zero. The principal optical difference appears when $\Delta\varphi$ and ϕ increase: the Bragg reflection pattern reoccurs an infinite numbers of times due to the periodic definition of the parameters of the TGBA phase.

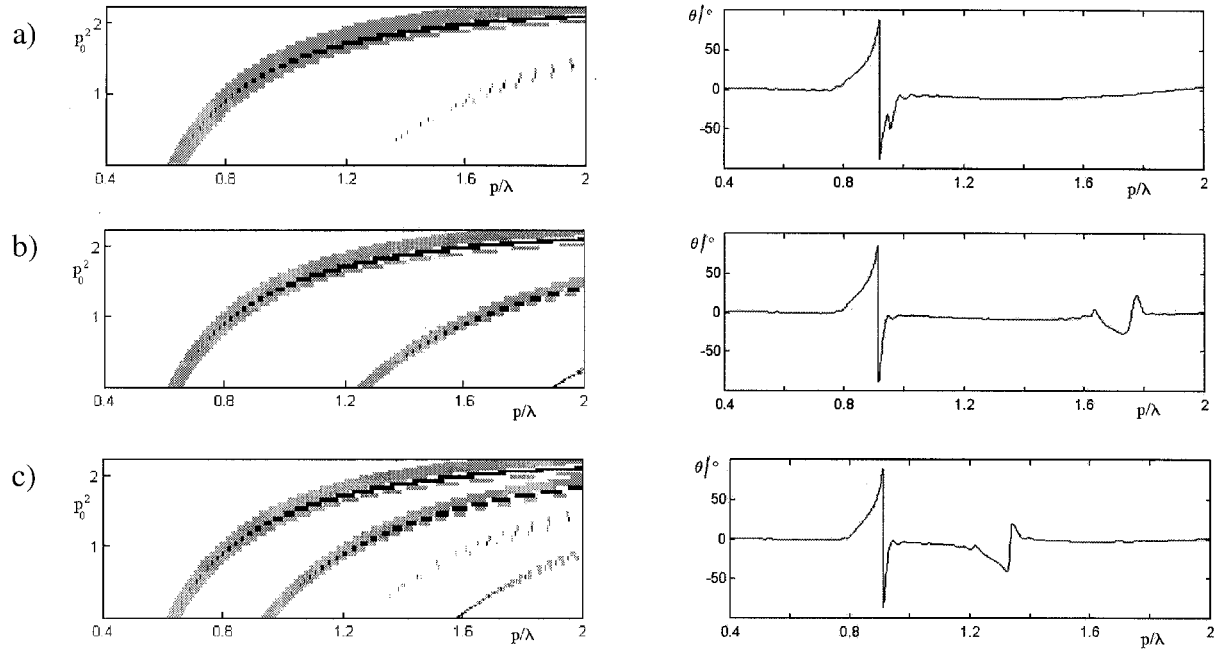

Figure 6. Chart of stability for the TGBA phase as a function of p_0^2 and p/λ (left side), and of rotation angle θ for an incidence of 45° as a function of p/λ (right side) with $p = 0.3$ μm, $d = 10p$ and $N_p = 20$, 4, 3 for (*a*), (*b*) and (*c*), respectively.

The author gratefully acknowledges Prof. Claudio Oldano for fruitful discussions.

References

[1] Goodby, J. W., Waugh, M. A., Stein, S. M., Chin, E., Pindak, R., and Patel, J. S., 1989, *Nature*, **337,** 449.
[2] Barois, P., Nobili, M., and Petit, M., *Mol. Cryst. Liq. Cryst* (to be published).
[3] Pramod, P. A., Pratiba, R., and Madhusudana, N. V., 1997, *Curr. Sci.*, **73,** 761.
[4] Renn, S. R., and Lubensky, T. C., 1988, *Phys. Rev. A*, **38,** 2132; Lubensky, T. C., and Renn, S. R., 1990, *Phys. Rev. A*, **41,** 4392.
[5] Renn, S. R., 1992, *Phys. Rev. A*, **45,** 953.
[6] De Gennes, P. G., 1972, *Solid State Commun.*, **10,** 753.
[7] Nguyen, H. T., Bouchta, A., Navailles, L., Barois, P., Isaert, N., Tweig, R. J., Maaroufi, A., and Destrade, C., 1992, *J. Phys. II Fr.*, **2,** 1889.
[8] Ihn, K. J., Zasadzinski, J. A. N., Pindak, R., Slaney, A. J., and Goodby, J. W., 1992, *Science*, **258,** 275.
[9] Navaille, L., Barois, P., and Nguyen, H. T., 1993, *Phys. Rev. Lett.*, **71,** 545.
[10] Andal, N., and Ranganath, G. S., 1995, *J. Phys. II Fr.*, **5,** 1193.
[11] Jolly, G., and Billard, J., 1981, *J. Opt. (Paris)*, **12,** 323; Jolly, G., and Billard, J., 1982, *J. Opt. (Paris)*, **13,** 227; Jolly, G., and Billard, J., 1985, *J. Opt. (Paris)*, **16,** 203; Jolly, G., and Billard, J., 1986, *J. Opt. (Paris)*, **17,** 211.
[12] Yariv, A., and Yeh, P., 1984, *Optical Waves in Crystals* (New York: John Wiley & Sons).
[13] Berreman, D. W., 1972, *J. opt. Soc. Am.*, **62,** 502.
[14] Altman, C., and Suchy, K., 1991, *Reciprocity, Spatial Mapping and Time Reversal in Electromagnetics* (Dordrecht: Kluver Academic Publishers).
[15] Reese, P. S., and Lakhtakia, A., 1990, *Optik*, **86,** 47.
[16] Oldano, C., Miraldi, E., Taverna Valabrega, P., 1983, *Phys. Rev. A*, **27,** 3291.
[17] Oldano, C., 1983, *Phys. Rev. A*, **27,** 3291.
[18] Hubert, P., Becchi, M., and Oldano, C. (unpublished results).
[19] De Vries, H., 1951, *Acta Crystallogr.*, **4,** 219.

Downloaded At: 19:09 25 January 2011